Supporting Information

A self-assembled Pd_2L_4 cage that selectively encapsulates nitrate

Lipeng Zhou, Qingfu Sun*

State Key Laboratory of Structural Chemistry, Fujian Institute of Research on the Structure of Matter, Chinese Academy of Sciences, Fuzhou 350002, P.R. China

Corresponding Email: qf-sun@fjirsm.ac.cn

Contents

1. General

2. Synthesis of ligand 1

• **Scheme S1** The synthetic route of ligand **1**.
• **Fig. S1** ^{1}H NMR spectrum of the ligand **1**.

3. Synthesis of complexes

• **Figs. S2** to **S8**: The characterization of **2a**.
• **Figs. S9** to **S15**: The characterization of **2b**.
• **Figs. S16** to **S23**: The characterization of **2c**.

4. The BF_4^- exchanged by NO_3^-

• **Figs. S24** and **S25**: The NMR characterization of anion exchange from BF_4^- to NO_3^-.

5. The BF_4^- exchanged by Cl^-

• **Figs. S26** and **S27**: The NMR characterization of anion exchange from BF_4^- to Cl^-.

6. The anion exchange experiment

• **Fig. S28**: The NMR characterization of anion exchange of **2c**.

7. The anion exchange kinetics experiment

• **Fig. S29 to S31**: The reaction kinetics of the anion exchange of **2c**

8. Single crystal X-ray diffraction study

•**Table S1**. Crystal data and refinement of complex **2a**.
• **Fig. S32**: Ortep-drawing of the crystal structure of **2a**.

Reference

1. General

Unless otherwise noted, all chemicals and solvents were purchased from commercial corporations and used without further purification. Deuterated solvents were purchased from Sigma-Aldrich Co. LLC.

NMR spectra were measured on a Bruker III (400 MHz) spectrometer. ESI-Q-TOF mass spectra were recorded on maXis 4G . The data analyses of ESI-Q-TOF mass spectra were processed on a Bruker Data Analysis (Version 4.0) software and the simulations were performed on a Bruker Isotope Pattern software. FT-IR spectra were collected on a Bruker VERTEX 70 spectrometer (using KBr pellets).

2. Synthesis of ligand 1

Scheme S1 The synthetic route of ligand **1**

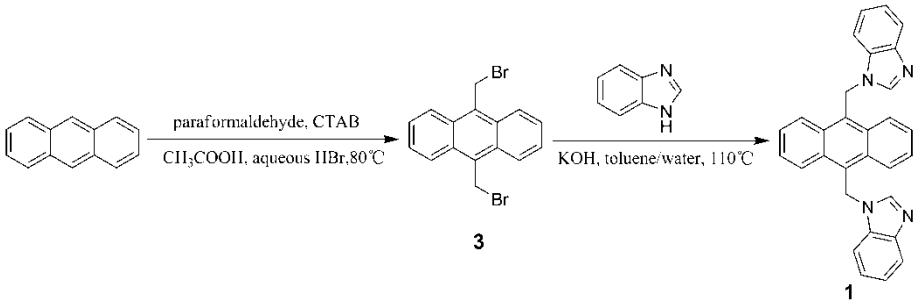

Synthesis of 9,10-Bis(bromomethyl)anthracene(3):

As per the procedure reported previously,[1] a mixture of anthracene (10g, 0.056 mmol, 1 equiv), paraformaldehyde (0.056 mmol), cetyltrimethylammoniumbromide (0.224 g), and glacial acetic acid (14 mL) were stirred at room temperature. Next, 35 mL of aqueous HBr (48 w%) was slowly added drop wise to the reaction mixture over a period of 1 h. The reaction mixture was stirred and heated to 80 °C for 5 h, cooled, filtered, washed with water, and then dried. Recrystallization from toluene furnished pure 9,10-bis(bromomethyl)anthracene. Yield 18.4 g (90%). All spectroscopic data matches the reported values.

Synthesis of 9,10-Bis(benzimidazol-1-ylthmethyl)anthracene(1)

9,10-Bis(benzimidazol-1-ylthmethyl)anthracene was synthesized according to a previous method.[2] A mixture of 9,10-bis(bromomethyl)anthracene (2 g, 5.49 mmol), benzimidazole (1.81 g, 15.32 mmol), aqueous KOH (10 M, 30 mL), toluene (60 mL), and Bu_4NOH (40%, 5 drops) was stirred and refluxed for 10 h. The mixture was cooled, filtered, then diluted with H_2O (100 mL) and the organic layer separated, dried over $MgSO_4$ and concentrated before purification by recrystallization from chloroform/hexane (1 : 1). Yield 1.99 g (82%). All spectroscopic data matches the reported values.

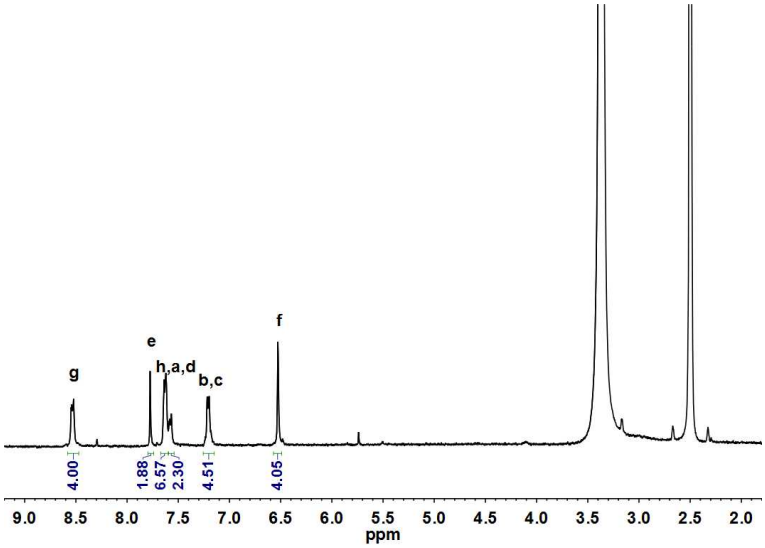

Fig. S1 ^{1}H NMR spectrum of the ligand **1** (400 MHz, d_6-DMSO, 298K)**.**

3. Synthesis of complexes

$(Pd_2L_4)(NO_3)_4$ (2a) : Ligand **1** (7.93 mg, 18.08 μmol) was treated with $Pd(NO_3)_2$ (9.05 μmol) in DMSO (0.7 mL) at 70 °C for 2 h. ^{1}H NMR confirmed the quantitative formation of complex. m.p.> 300 °C. ^{1}H NMR (400 MHz, d_6-DMSO) δ 8.69 (d, J = 9.2 Hz, H_a, 2H), 8.25 (d, J = 8.2 Hz, H_{g1}, 2H), 8.05 – 7.87 (t, H_b, 2H), 7.78 (dt, J = 4.1 Hz, H_{h1}, 2H), 7.46 (dd, J = 3.9 Hz, H_{g2} and H_{h2}, 4H), 6.48 – 6.27 (m, H_d, H_{f1} and H_{f2}, 6H), 6.06 (s, H_e, 2H), 5.48 (t, J = 7.7 Hz, H_c, 2H). ^{13}C NMR (100 MHz, d_6-DMSO) δ 142.45, 139.03, 132.78, 129.29, 128.77, 126.66, 125.60, 125.50, 125.24, 124.76, 124.27, 122.71, 116.51, 113.55, 42.687.ESI: *m/z* Calcd for $[(NO_3 \subset \mathbf{2})]^{3+}$ 676.1786, found 676.1450; Calcd for $[(NO_3 \subset \mathbf{2})\cdot NO_3]^{2+}$ 1045.2621, found 1045.2105. After anion exchange with $NaBF_4$, Calcd for $[(NO_3 \subset \mathbf{2})]^{3+}$ 676.1786, found 676.1837; Calcd for $[(NO_3 \subset \mathbf{2})\cdot BF_4]^{2+}$ 1057.7701, found 1057.7762; Calcd for $[(NO_3 \subset \mathbf{2})\cdot 2BF_4]^{2+}$ 2202.5445, found 2202.5594.

$(Pd_2L_4)(BF_4)_4$ (2b) : Ligand **1** (7.93 mg, 18.08 μmol) was treated with $Pd(CH_3CN)_4(BF_4)_2$ (9.05 μmol) in DMSO (0.7 mL) at 110 °C for 2 h or at 80 °C for 24 h. ^{1}H NMR confirmed the quantitative formation of complex. m.p.> 300 °C. ^{1}H NMR (400 MHz, d_6-DMSO) δ 8.70 (d, J = 9.1 Hz, H_a, 2H), 8.25 (d, J = 8.2 Hz, H_{g1}, 2H), 8.10 (t, J = 7.4 Hz,H_b 2H), 7.78 (m, H_{g2} and H_{h1}, 4H), 7.51 (t, J = 7.8 Hz, H_{h2}, 2H), 6.51 – 6.13(m, H_d, H_{f1} and H_{f2}, 6H),, 5.97 (s, H_e, 2H), 5.71 (t, J = 8.0 Hz, H_c, 2H). ^{13}C NMR (101 MHz, DMSO) δ 140.96, 138.72, 132.31, 128.77, 128.71, 126.02, 125.21, 125.00, 124.66, 124.62, 124.00, 122.55, 116.57, 113.04, 42.54. ESI: *m/z* Calcd for $[(BF_4 \subset \mathbf{2})]^{3+}$ 684.5173, found 684.5360; Calcd for $[(BF_4 \subset \mathbf{2})\cdot BF_4]^{2+}$ 1070.2781, found 1070.2933; Calcd for $[(BF_4 \subset \mathbf{2})\cdot 2BF_4]^{+}$ 2227.5604, found 2227.4667.

$(Pd_2L_4)(PF_6)_4$ (2c) : $PdCl_2$ (17.73 mg, 0.10 mmol) was dissolved in DMSO (2 mL) and stirred for 1 h at room temperature with AgPF6 (50.57 mg, 0.20 mmol). After removal of AgCl by filtration, $Pd(PF_6)_2$ was first prepared. Then ligand **1** (7.93 mg, 18.08 μmol) was treated with $Pd(PF_6)_2$ (9.05 μmol) in DMSO (0.7 mL) at 70 °C for 2 h. ^{1}H NMR confirmed the quantitative formation of complex. m.p.> 300 °C. ^{1}H NMR (400 MHz, d_6-DMSO) δ 8.73 (d, J = 9.1 Hz, H_a, 2H), 8.24 (d, J = 8.1 Hz, H_{g1}, 2H), 7.81 (dt, J = 7.1 Hz, H_b and H_{h1},4H), 7.55 – 7.46 (m, H_{g2} and H_{h2}, 4H), 6.56 – 6.31 (m, H_d, H_{f1} and H_{f2}, 6H), 5.95 (s, H_e, 2H), 5.35 (t, J = 7.8 Hz, H_c, 2H). ^{13}C NMR (100 MHz, d_6-DMSO) δ 141.99, 139.11, 133.14, 129.22, 128.36, 127.04, 125.55, 125.42, 125.31, 125.17, 123.57, 122.61, 116.86, 113.36, 42.59.

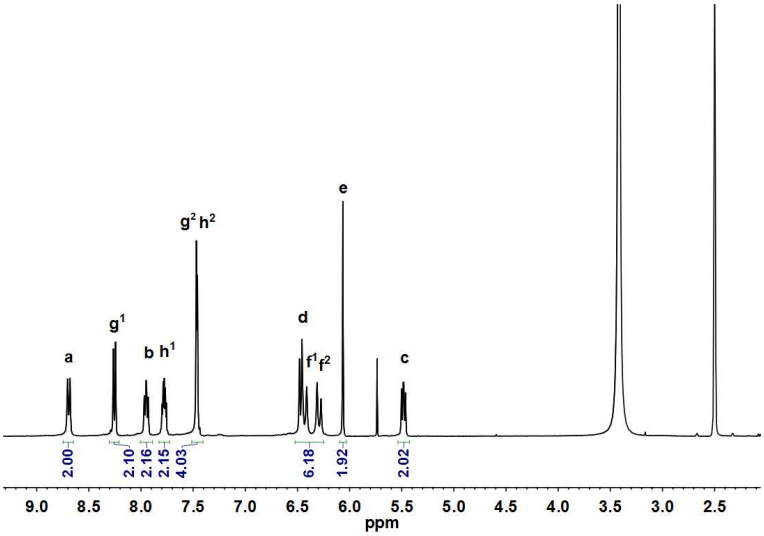

Fig. S2 ^{1}H NMR spectrum of the complex **2a** (400 MHz, d_6-DMSO, 298K)**.**

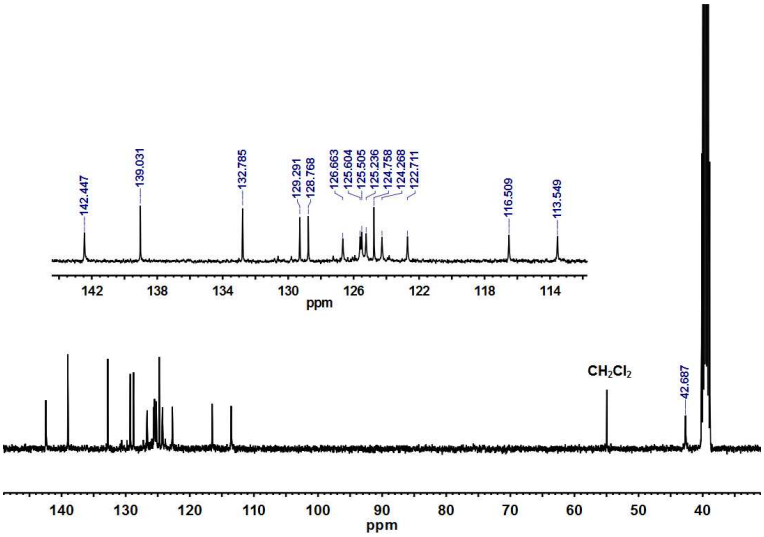

Fig. S3 ^{13}C NMR spectrum of the complex **2a** (100 MHz, d_6-DMSO, 298K)**.**

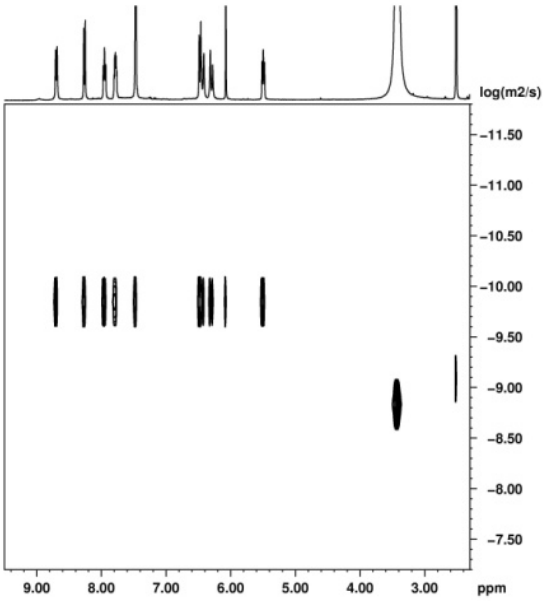

Fig. S4 ^{1}H DOSY spectrum of the complex **2a** (400 MHz, d_6-DMSO, 298K)**.**

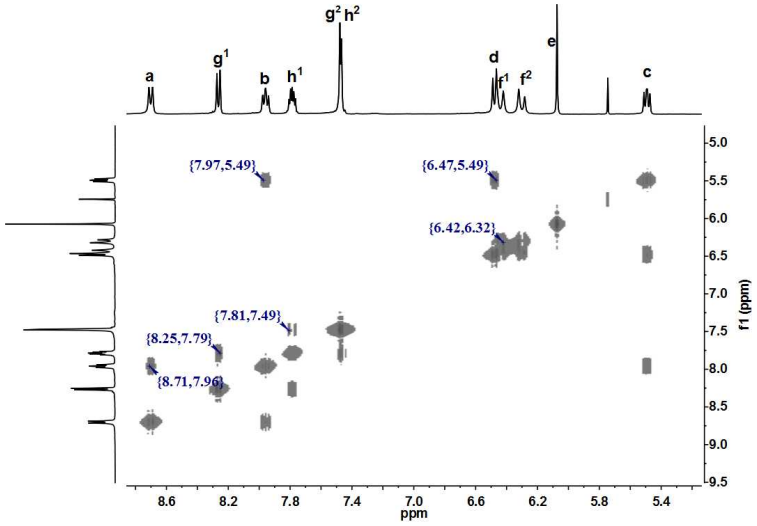

Fig. S5 ^{1}H-^{1}H COSY NMR spectrum of the complex **2a** (400 MHz, d_6-DMSO, 298K)**.**

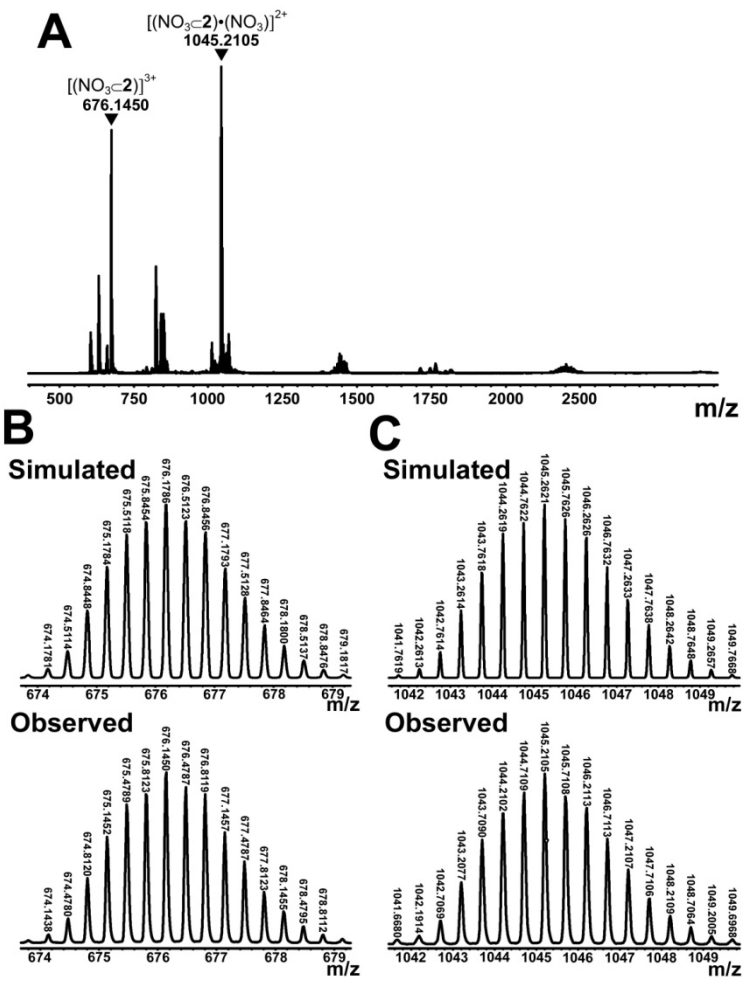

Fig. S6 A) HR-Mass spectrum of complex **2a**; B) and C) simulated and observed isotopic distribution of the trivalent peaks $[(NO_3 \subset \mathbf{2})]^{3+}$ and the divalent peaks $[(NO_3 \subset \mathbf{2})\cdot BF_4]^{2+}$.

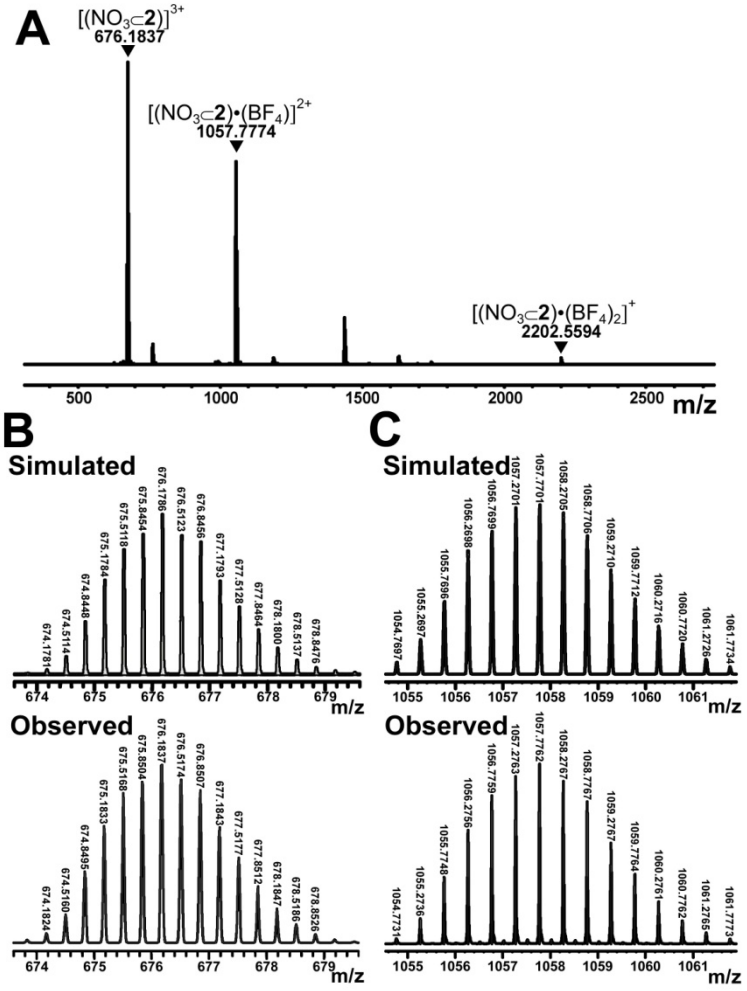

Fig. S7 A) HR-Mass spectrum of complex **2a** after anion exchange with $NaBF_4$; B) and C) simulated and observed isotopic distribution of the trivalent peaks $[(NO_3 \subset \mathbf{2})]^{3+}$ and the divalent peaks $[(NO_3 \subset \mathbf{2})\cdot BF_4]^{2+}$.

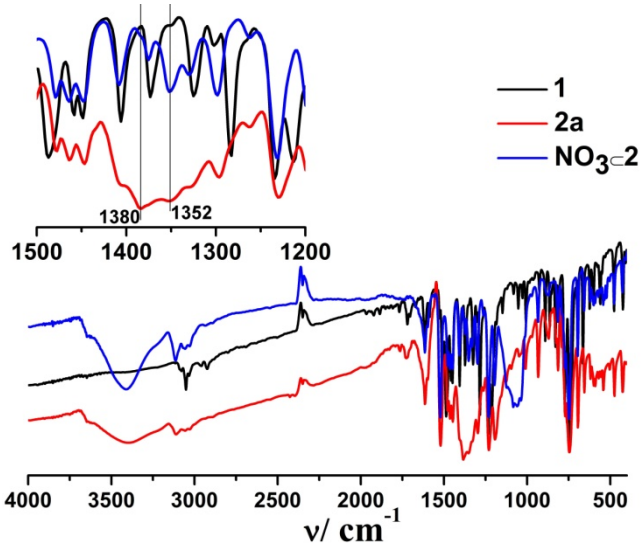

Fig. S8 IR spectrum of the ligand **1** (black curve), the complex **2a** (red curve) and the complex $[(NO_3 \subset \mathbf{2})\cdot 3BF_4]$ after anion exchange with $NaBF_4$ (blue curve). The peak at 1380 and 1352 cm^{-1}

represent the free and encapsulated nitrate.

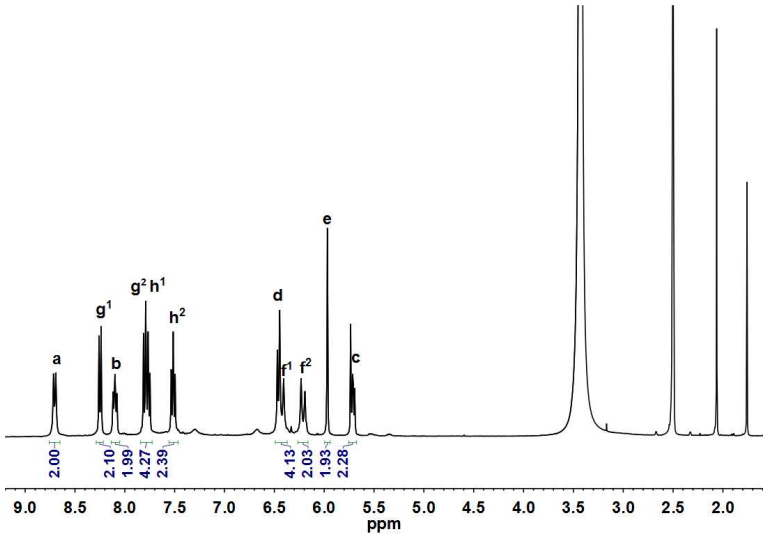

Fig. S9 ^{1}H NMR spectrum of the complex **2b** (400 MHz, d_6-DMSO, 298K)**.**

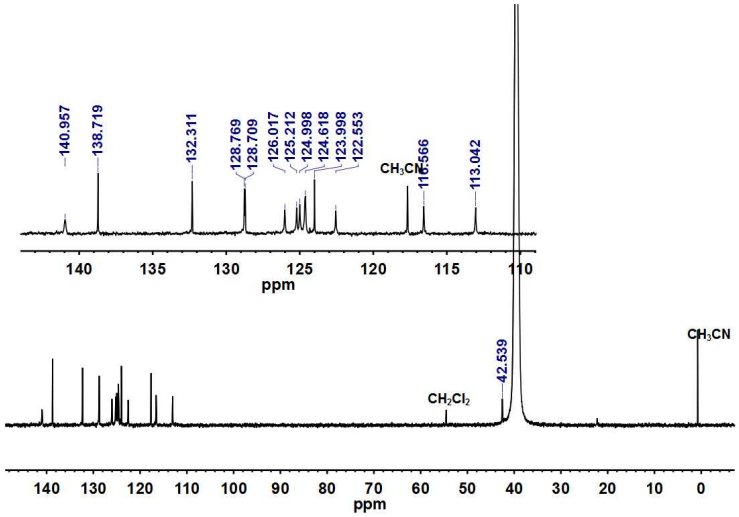

Fig. S10 ^{13}C NMR spectrum of the complex **2b** (100 MHz, d_6-DMSO, 298K)**.**

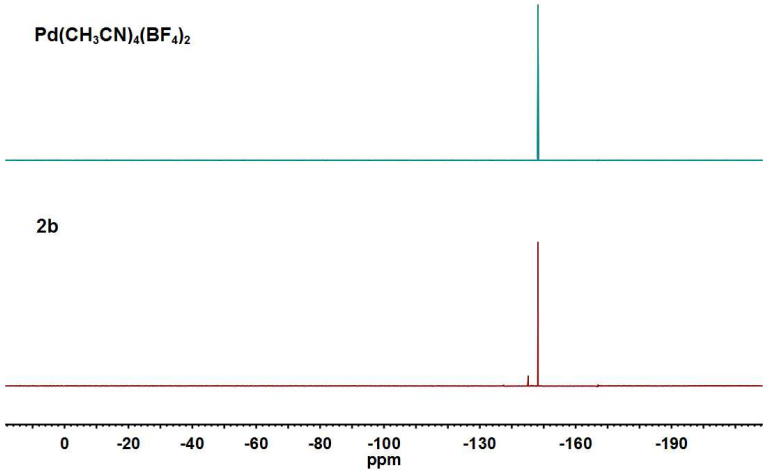

Fig. S11 ^{19}F NMR spectrum of the complex **2b** (376 MHz, d_6-DMSO, 298K)**.**

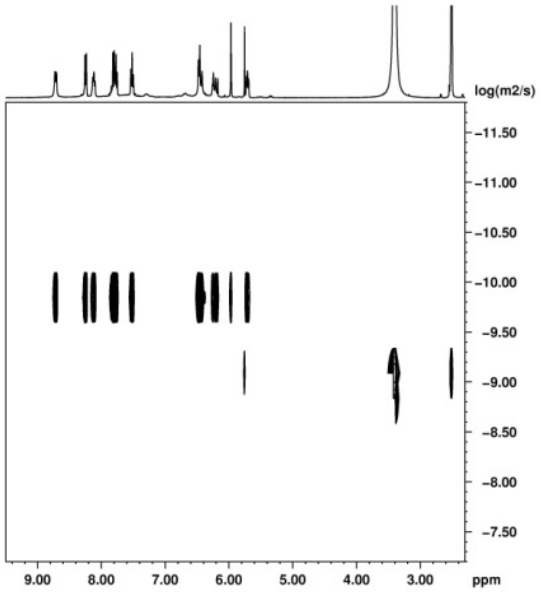

Fig. S12 ^{1}H DOSY spectrum of the complex **2b** (400 MHz, d_6-DMSO, 298K)**.**

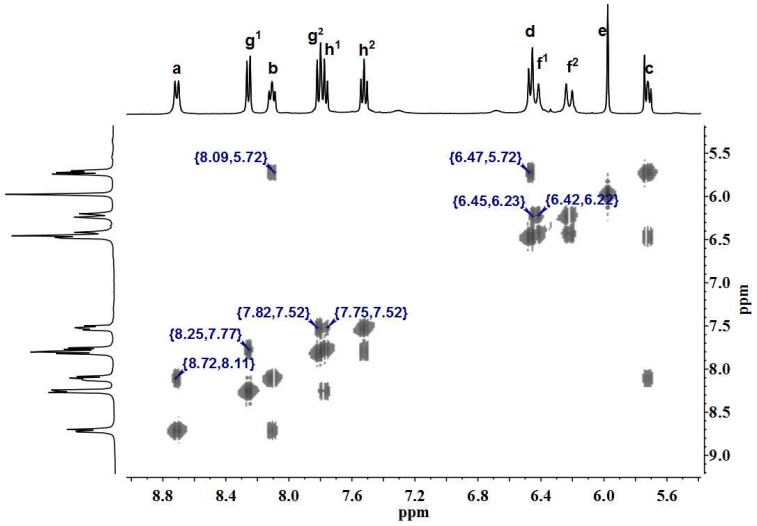

Fig. S13 ^{1}H-^{1}H COSY NMR spectrum of the complex **2b** (400 MHz, d_6-DMSO, 298K).

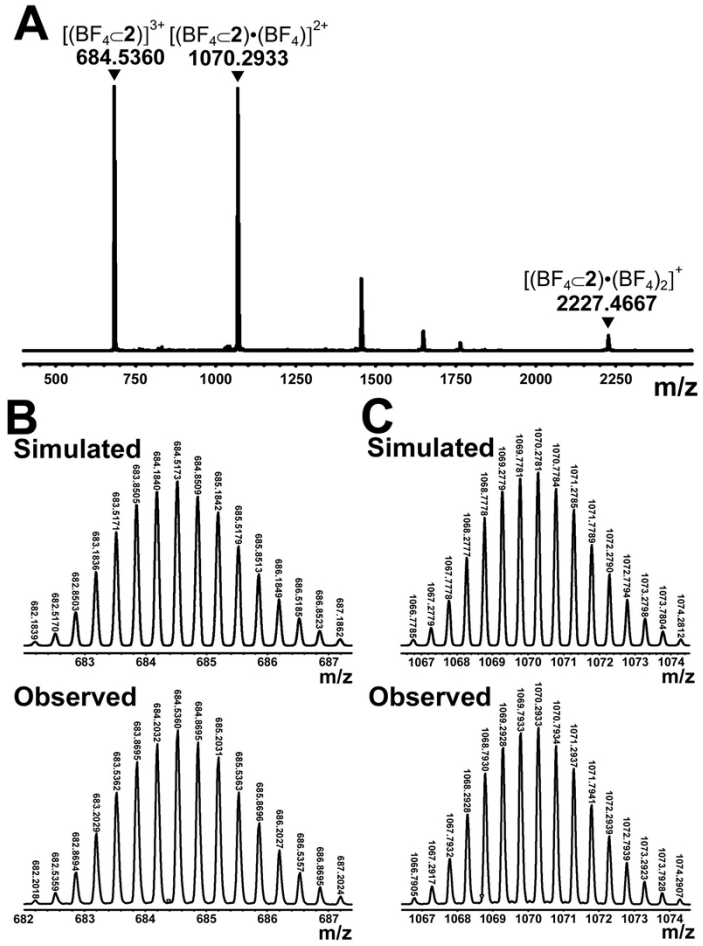

Fig. S14 A) HR-Mass spectrum of complex **2b**; B) and C) simulated and observed isotopic distribution of the trivalent peaks $[(BF_4 \subset \mathbf{2})]^{3+}$ and the divalent peaks $[(BF_4 \subset \mathbf{2})\cdot BF_4]^{2+}$.

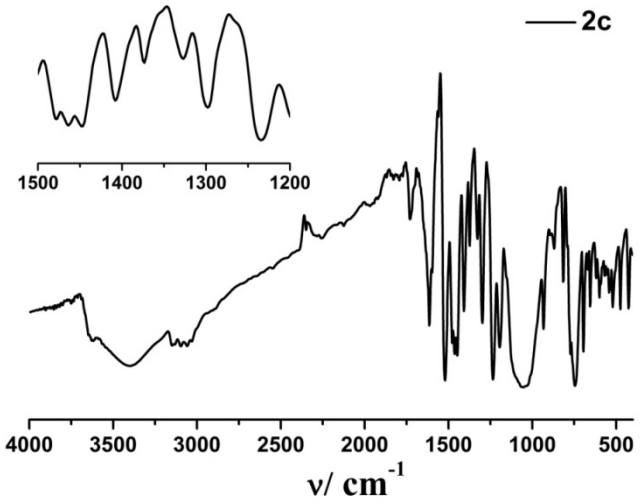

Fig. S15 IR spectrum of the complex **2b.**

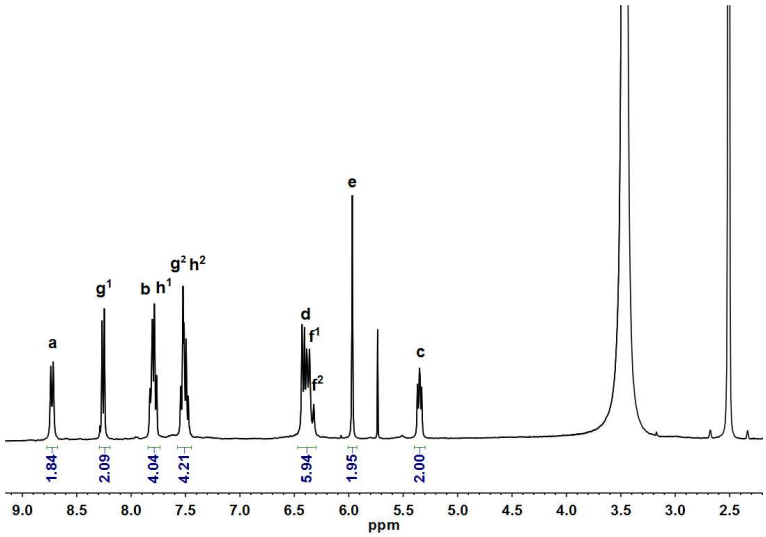

Fig. S16 ^{1}H NMR spectrum of the complex **2c** (400 MHz, d_6-DMSO, 298K)**.**

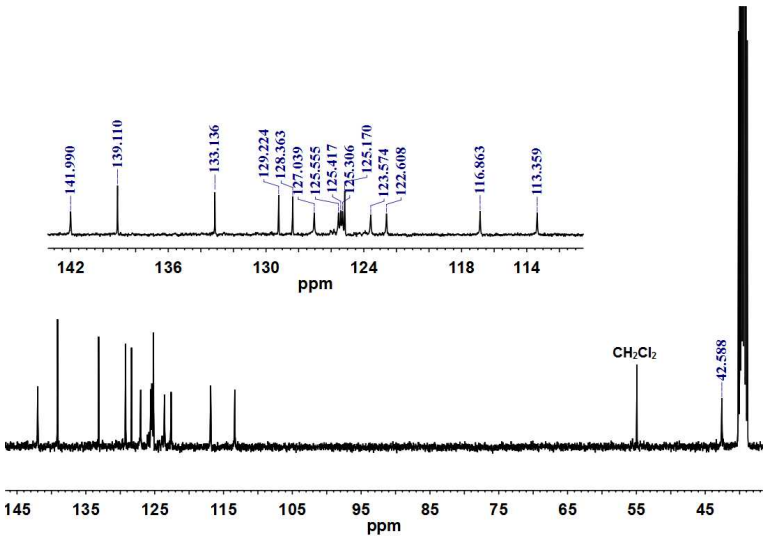

Fig. S17 ^{13}C NMR spectrum of the complex **2c** (100 MHz, d_6-DMSO, 298K)**.**

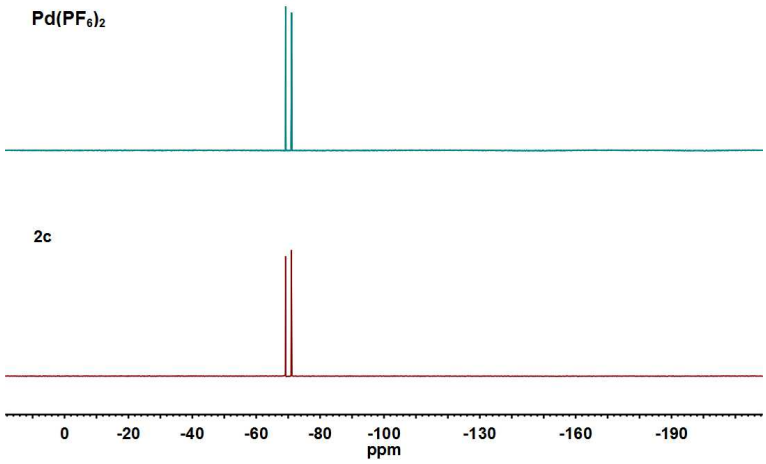

Fig. S18 ^{19}F NMR spectrum of the complex **2c** (376 MHz, d_6-DMSO, 298K)**.**

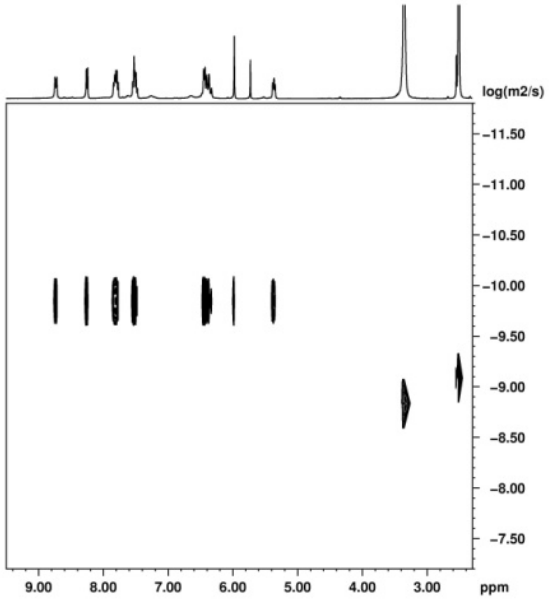

Fig. S19 ^{1}H DOSY spectrum of the complex **2c** (400 MHz, d_6-DMSO, 298K)**.** (logD=- 9.879)

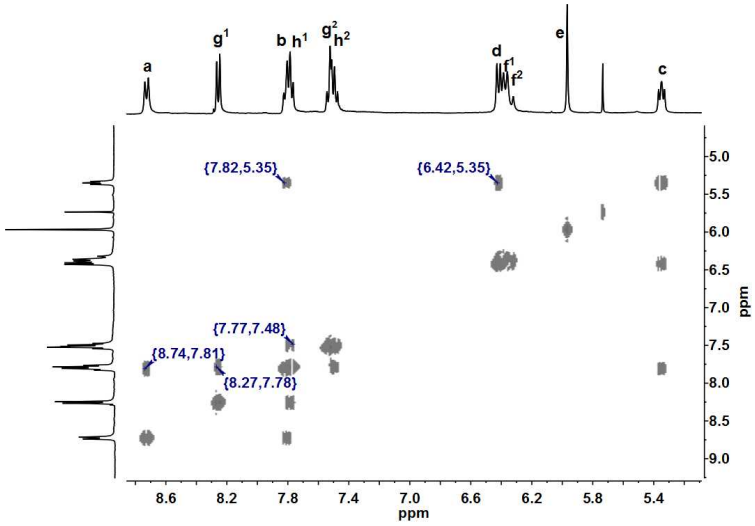

Fig. S20 ^{1}H-^{1}H COSY NMR spectrum of the complex **2c** (400 MHz, d_6-DMSO, 298K)**.**

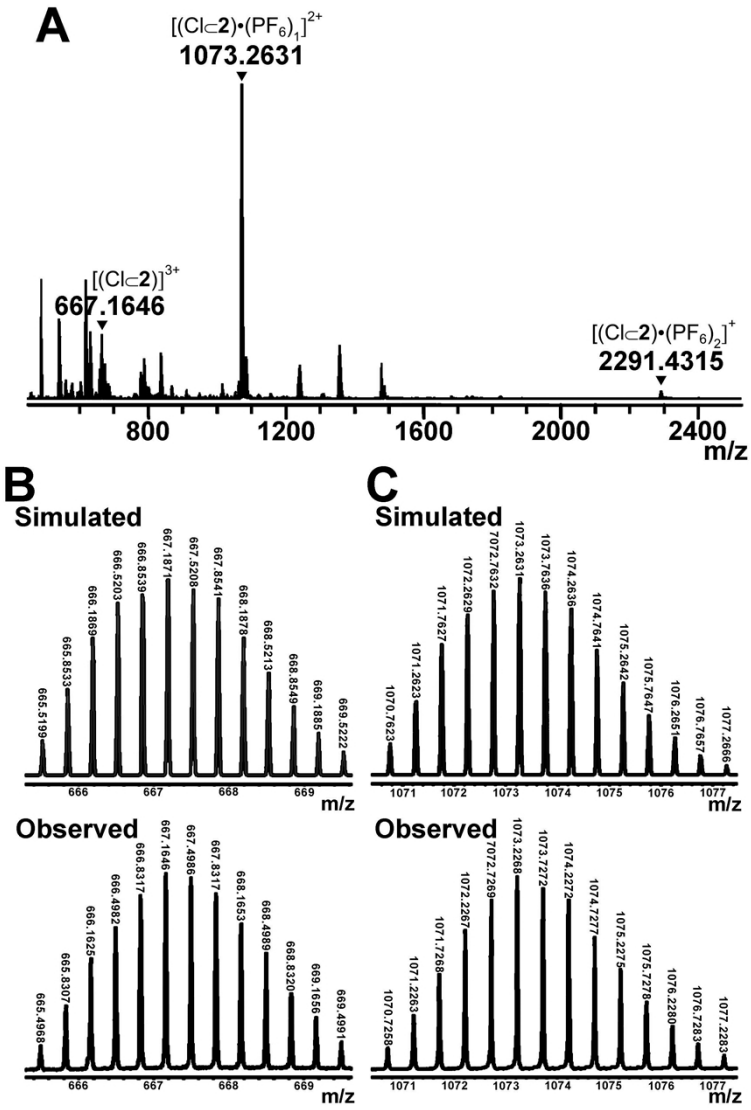

Fig. S21 A) HR-Mass spectrum of complex **2c**; B) and C) simulated and observed isotopic distribution of the trivalent peaks $[(Cl \subset \mathbf{2})]^{3+}$ and the divalent peaks $[(Cl \subset \mathbf{2})\cdot PF_6]^{2+}$.

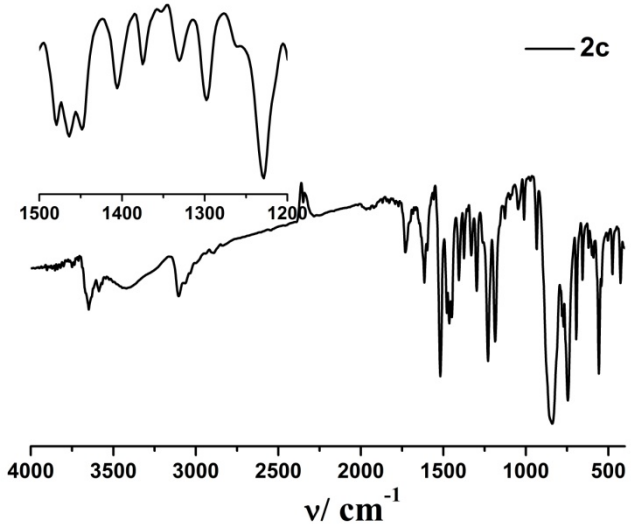

Fig. S22 IR spectrum of the complex **2c.**

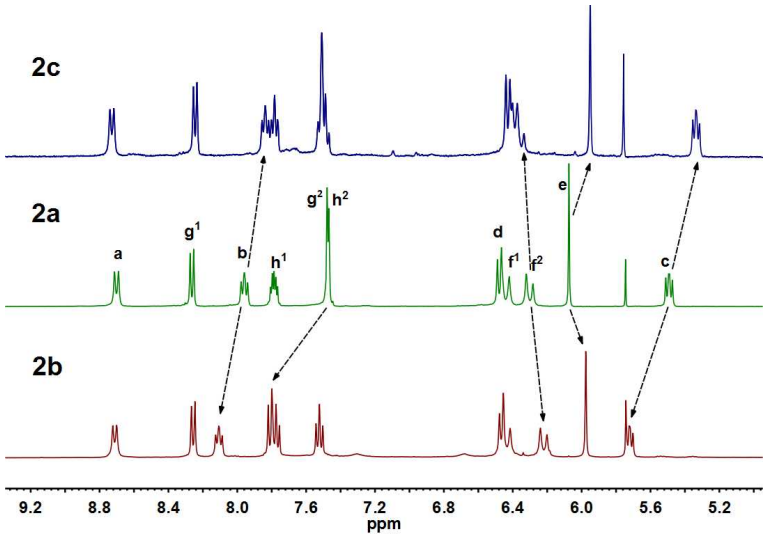

Fig. S23 ^{1}H NMR spectrum of the complex **2a, 2b and 2c** (400 MHz, d_6-DMSO, 298K)**.**

4. The BF_4^- exchanged by NO_3^-

0.5 and 1 equivalent (versus cage) of KNO_3 were added into the prepared solution of cage **2b,** respectively, followed by stirred for 10 h at 110 ℃. The ^{1}H and ^{19}F NMR spectra revealed the anion exchange accomplished.

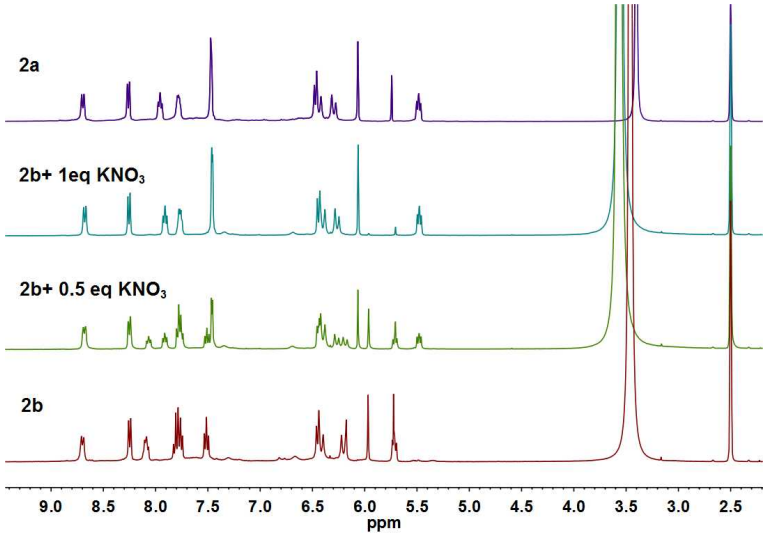

Fig. S24 ^{1}H NMR spectrum of complex **2b** after the addition of 0.5 equivalent and 1.0 equivalent of KNO_3, respectively (400 MHz, d_6-DMSO, 298K).

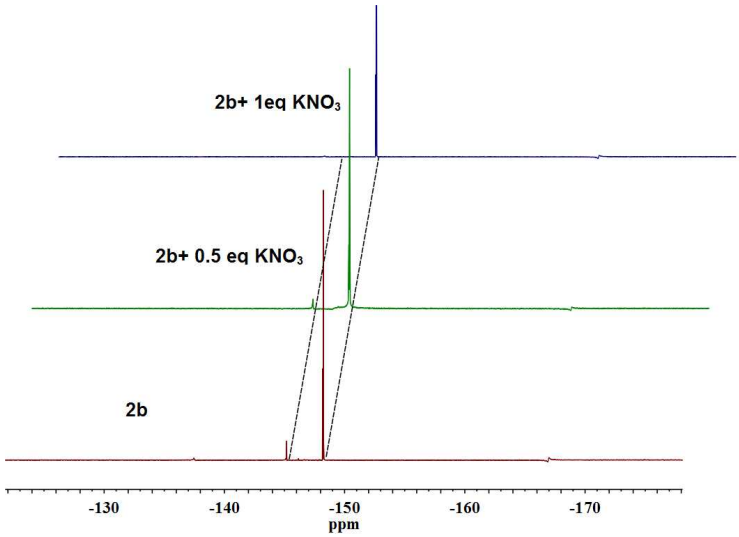

Fig. S25 ^{19}F NMR spectrum of complex **2b** after the addition of 0.5 equivalent and 1.0 equivalent of KNO_3 , respectively (376 MHz, d_6-DMSO, 298K).

5. The BF_4^- exchanged by Cl^-

1.2 equivalent (versus cage) of $N(C_4H_9)_4Cl$ was added into the prepared solution of cage **2b,** followed by stirred for 24 h at 110 ℃. The ^1H and ^{19}F NMR spectra revealed that about 87.3% of BF_4^- exchanged by Cl^-.

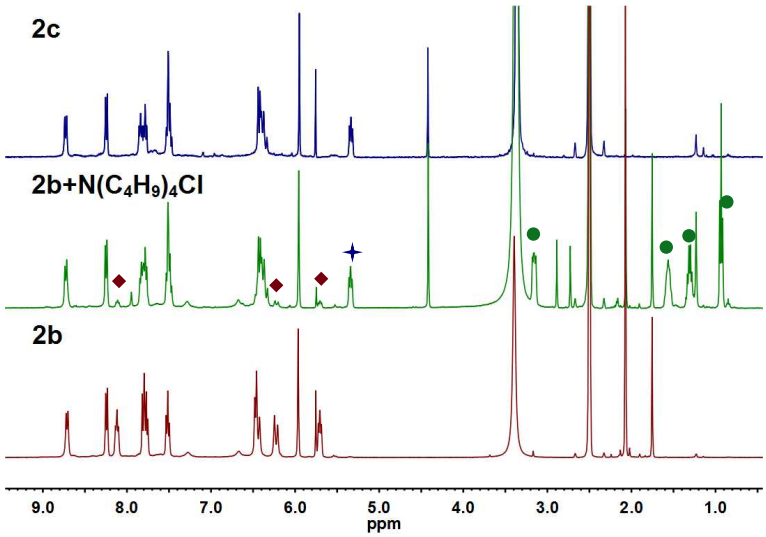

Fig. S26 ^1H NMR spectrum of complex **2b** after the addition of 1.2 equivalent of $N(C_4H_9)_4Cl$ (400 MHz, d_6-DMSO, 298K). Resonances corresponding to **2b**, **2c**, and $N(C_4H_9)_4^+$ are marked by ◆, ✦, and ● ,respectively..

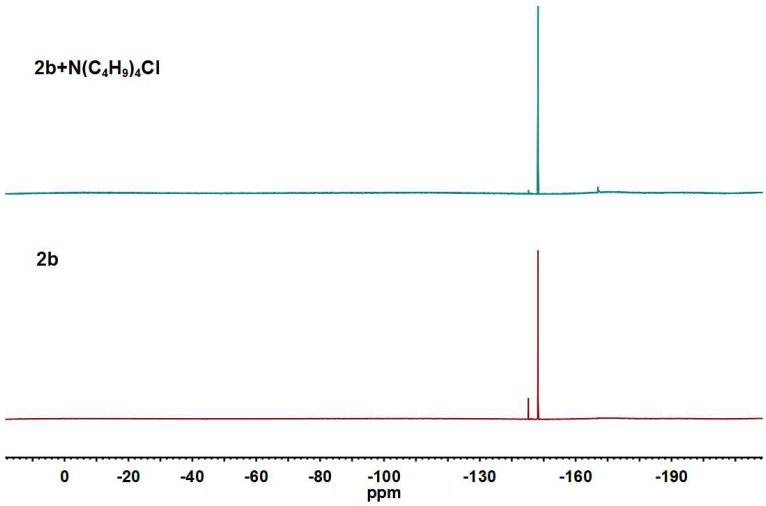

Fig. S27 ^{19}F NMR spectrum of complex **2b** after the addition of 1.2 equivalent of $N(C_4H_9)_4Cl$ (376 MHz, d_6-DMSO, 298K).

6. The anion exchange experiment

1.1 equivalent (versus cage) of different salts were added into the prepared free cage **2c,** followed by stirred for 20 h at 70 ℃ except $NaBF_4$ for 20 h at 110 ℃. For F^-, $CF_3SO_3^-$, CO_3^-, CH_3COO^- (Ac^-), $H_2PO_4^-$, HSO_4^-, etc, no signals refered to the anion-cage complex were observed. For NO_3^-, NO_2^-, Br^-, I^- and BF_4^-, new peaks appeared (at 6.07 ppm, 6.07 ppm, 6.07ppm, 5.51 ppm and 5.71 ppm, respectively), which was the evidence of the anion exchange. The concentrations of occupied and unoccupied cage were determined by integrating the ^1H NMR spectra using nitromethane as the internal standard. The equilibrium constants were further obtained by calculation.

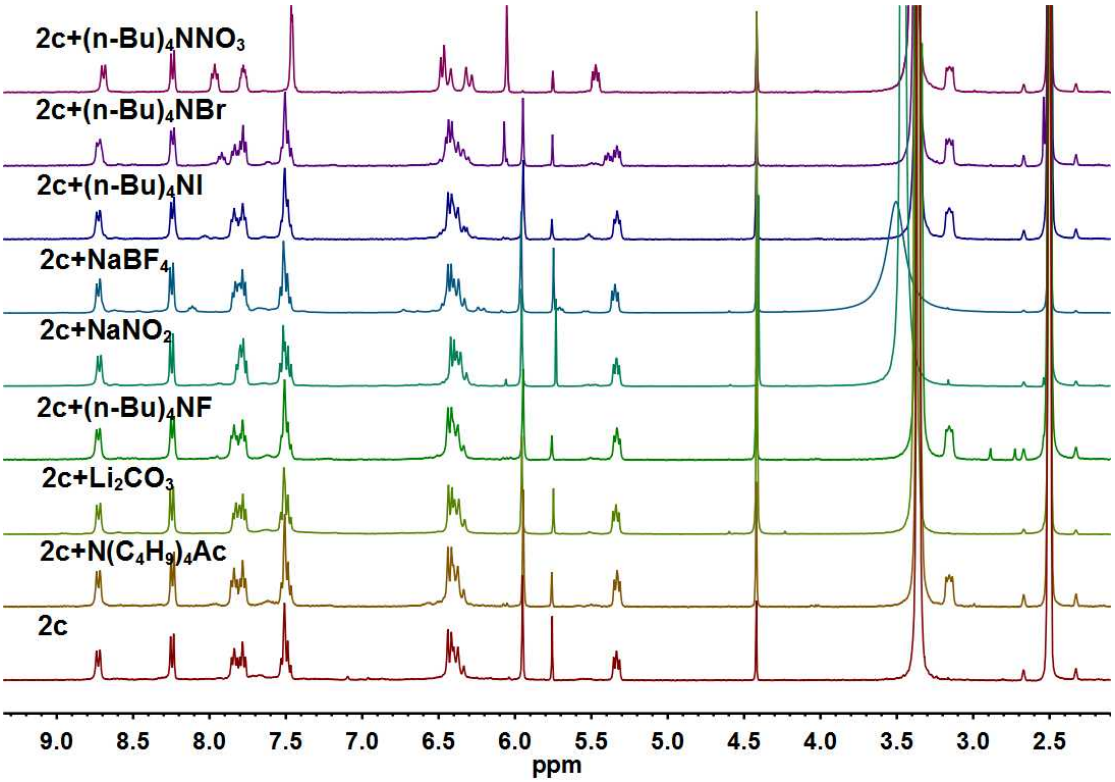

Fig. S28 ^{1}H NMR spectrum of complex **2c** plus 1.1 equivalent of anions (400 MHz, d_6-DMSO, 298K).

7. The anion exchange kinetics experiment

$(n\text{-}C_4H_9)_4NBr$ or $(n\text{-}C_4H_9)_4NNO_3$ (1.0 equivalent versus cage) was added into the prepared cage **2c**, respectively, followed by stirred at 70 ℃. The ^{1}H NMR spectrum were recorded at different time. The conversion ratios were determined by the integration of the characteristic encapsulation signals (6.07 ppm) in the ^{1}H NMR experiments.

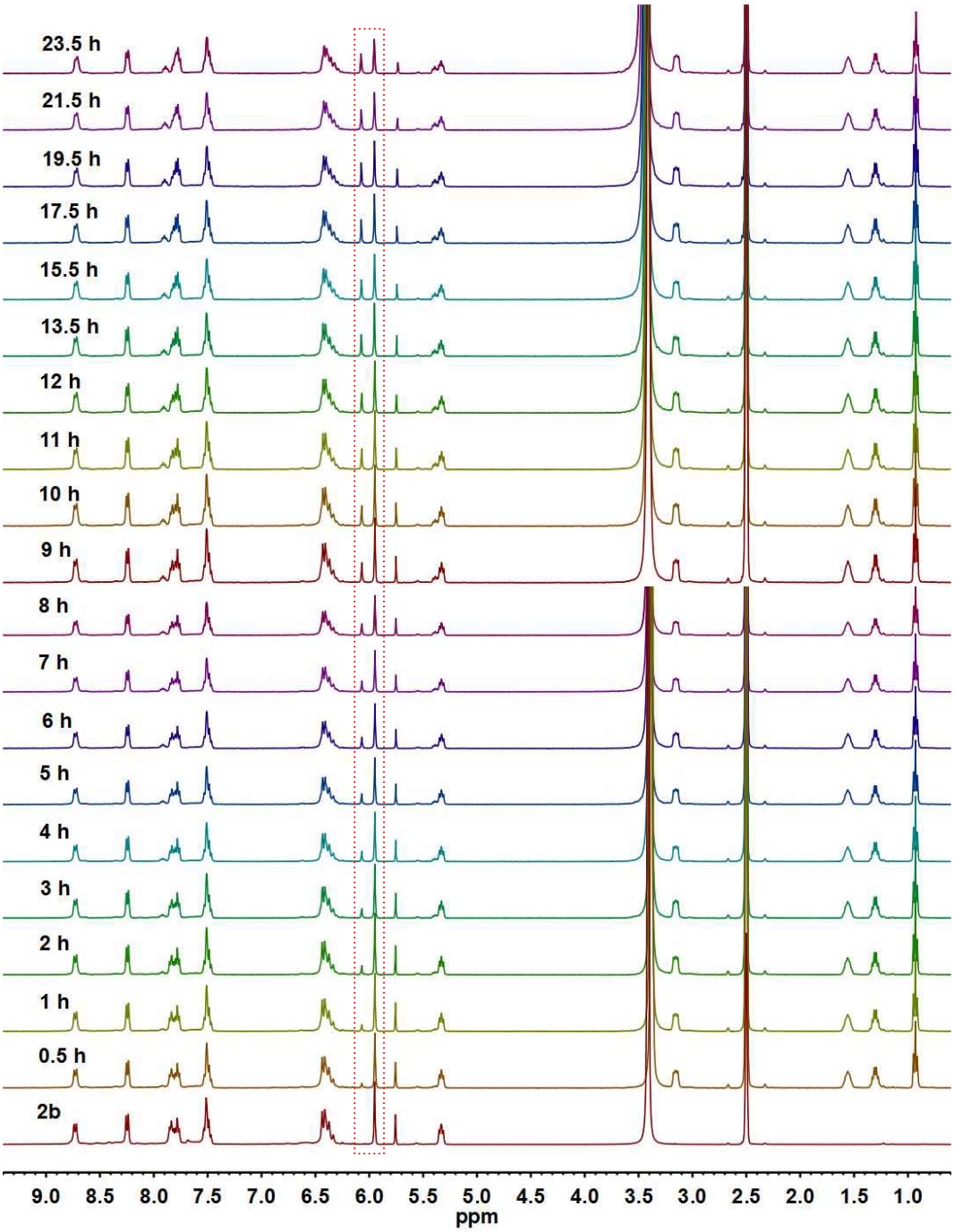

Fig. S29 ^{1}H NMR spectrum of complex **2c** plus 1.0 equivalent of $(n\text{-}C_4H_9)_4NBr$ stirred at 70 ℃ for different time (400 MHz, d_6-DMSO, 298K).

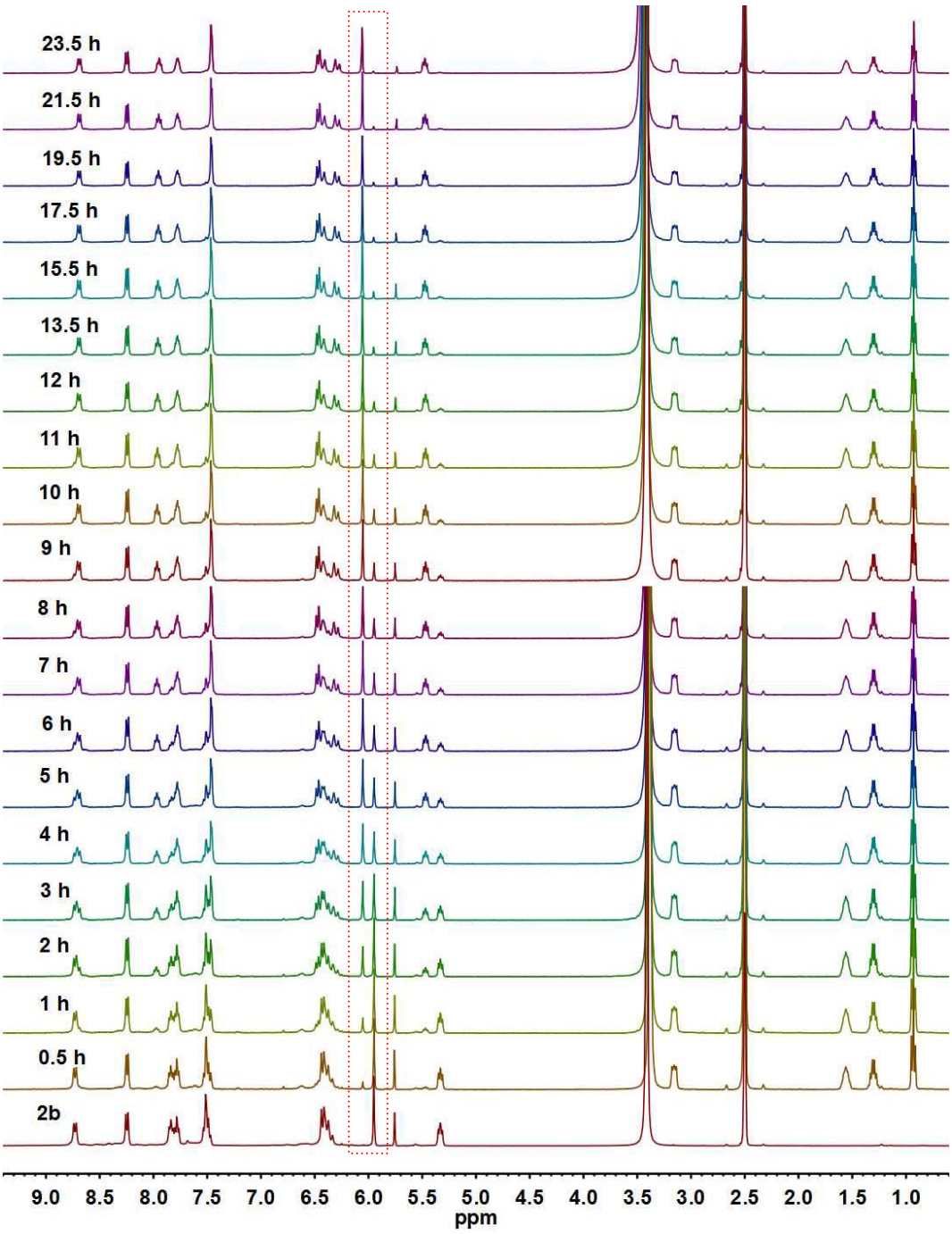

Fig. S30 ^{1}H NMR spectrum of complex **2c** plus 1.0 equivalent of $(n\text{-}C_4H_9)_4NNO_3$ stirred at 70 ℃ for different time (400 MHz, d_6-DMSO, 298K).

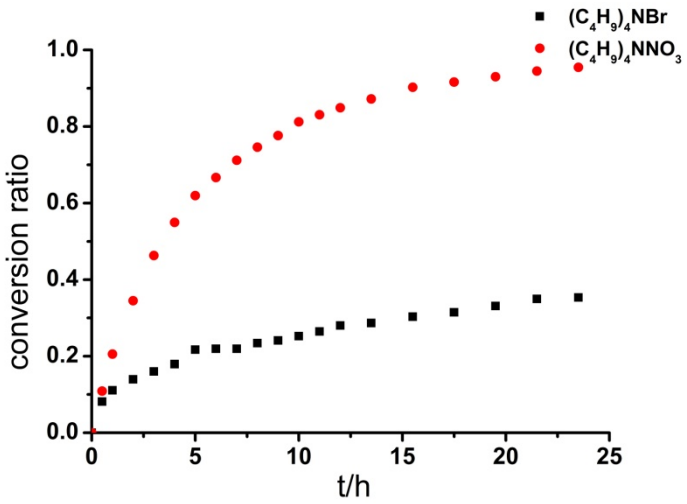

Figure 31. The reaction kinetics of the anion encapsulation of **2c** at 70°C. The conversion ratios were determined by the integration of the characteristic encapsulation signals in the ^{1}H NMR spectra.

8. Single crystal X-ray diffraction study

Crystals suitable for analysis by X-ray diffraction grew at room temperature over one weeks by gas phase diffusion of ethyl acetate or 1,4-dioxane into a DMSO solution of the complex **2a**.

For the single crystal analysis, a yellow crystal was taken directly from the mother liquor, transferred to oil and mounted into loop. The crystal was kept at 100.00(10) K during data collection on a supernova diffractometer equipped with a Multilayers mirror Cu-Kα radiation (λ = 1.5418 Å) by using a ω scan mode. The crystal structure was solved by direct method and refined by full-matrix least squares on F^2 using *SHELXTL* package.[S3] Part of non-hydrogen atoms were refined with anisotropic displacement parameters. The free solvent molecules are highly disordered, and attempts to locate and refine the solvent peaks were unsuccessful. The diffused electron densities resulting from these solvent molecules were removed using the *SQUEEZE* routine of *PLATON*;[S4] structures were then refined again using the data generated.

Crystal data for **2a**: Space group C_2, a = 13.7980 (14) Å, b = 32.546 (4) Å, c = 13.7267 (16) Å, α = 90°, β = 100.330 (10)°, γ = 90°. V = 6064.3 (12) Å^3, Z = 2, T = 102 K. R_1 = 0.0971, wR_2 = 0.2481, Goodness of fit = 1.075.

Table S1. Crystal data and refinement of complex **2a**.

Empirical formula	C128 H104 N17 O7 Pd2	
Formula weight	2205.08	
Temperature	102 K	
Wavelength	1.54178 Å	
Crystal system	Monoclinic	
Space group	C2	
Unit cell dimensions	a = 13.7980(14) Å	α= 90°.
	b = 32.546(4) Å	β= 100.330(10)°.
	c = 13.7267(16) Å	γ = 90°.
Volume	6064.3(12) $Å^3$	
Z	2	
Density (calculated)	1.208 Mg/m^3	
Absorption coefficient	2.871 mm^{-1}	
F(000)	2278	
Crystal size	0.100 x 0.100 x 0.040 mm^3	
Theta range for data collection	3.528 to 73.628°.	
Index ranges	-16<=h<=16, -38<=k<=40, -15<=l<=16	
Reflections collected	12514	
Independent reflections	9026 [R(int) = 0.0424]	
Completeness to theta = 67.679°	99.3 %	
Refinement method	Full-matrix least-squares on F^2	
Data / restraints / parameters	9026 / 2331 / 685	
Goodness-of-fit on F^2	1.075	
Final R indices [I>2sigma(I)]	R1 = 0.0971, wR2 = 0.2481	
R indices (all data)	R1 = 0.1256, wR2 = 0.2950	
Absolute structure parameter	0.52(3)	
Extinction coefficient	n/a	
Largest diff. peak and hole	2.347 and -0.755 $e.Å^{-3}$	

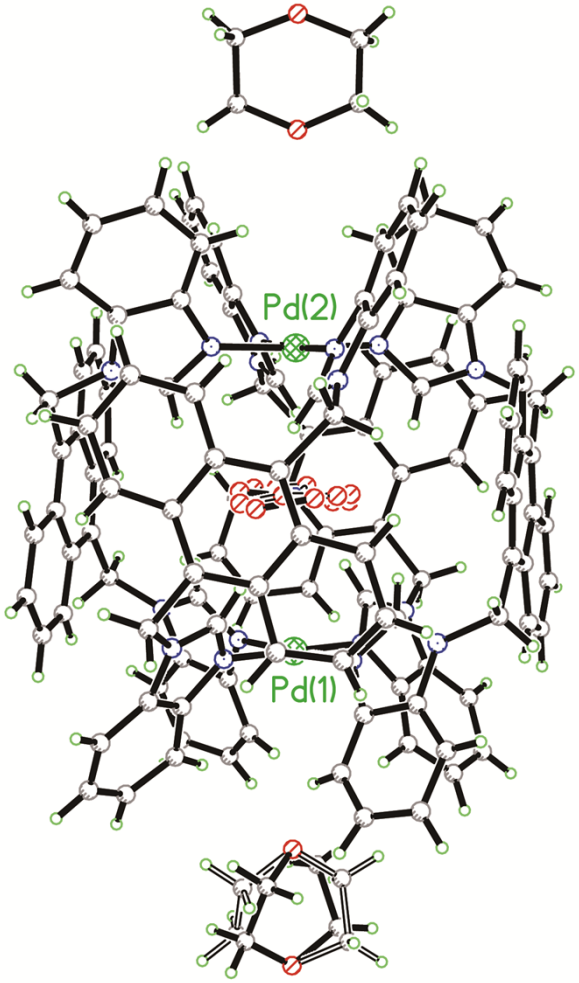

Fig. S32: Ortep-drawing of the crystal structure of **2a** at 30 % probability level.

References

S1. S. V. Aathimanikandan, B. S. Sandanaraj, C. G. Arges, C. J. Bardeen and S. Thayumanavan, *Org. Let.*, 2005, **7**, 2809-2812.

S2. J.-L. Du, T.-L. Hu, S.-M. Zhang, Y.-F. Zeng and X.-H. Bu, *CrystEngComm*, 2008, **10**, 1866.

S3. Sheldrick, G. M., *Acta Crystallogr. Sect. A*, 2008, **64**, 112-122.

S4. Spek, A. L., *J. Appl. Crystallogr.*, 2003, **36**, 7-13.